Syntheses, Structures, and Magnetism of Barium/Rare-Earth/Bismuth Double Perovskites. Crystal Structures of Ba_2MBiO_6 (M = Ce, Pr, Nd, Tb, Yb) by Powder Neutron Diffraction

William T. A. Harrison,[†,⊥] Kenneth P. Reis,[†,§] Allan J. Jacobson,[†,*] Lynn F. Schneemeyer,[‡] and Joseph V. Waszczak[‡]

Department of Chemistry, University of Houston, Houston, Texas 77204-5641, and AT&T Bell Laboratories, 600 Mountain Avenue, Murray Hill, New Jersey 07974

Received June 2, 1995. Revised Manuscript Received August 25, 1995[⊗]

The series of double perovskites Ba_2MBiO_6 (M = Ce to Lu) have been synthesized and characterized by chemical analysis and powder X-ray diffraction. The crystal structures of Ba_2MBiO_6 (M = Ce, Pr, Nd, Tb, Yb) have been determined by Rietveld analysis of powder neutron diffraction data. Magnetic susceptibility data for the compounds with M = Ce, Pr, Nd, and Tb are reported. In Ba_2CeBiO_6, the octahedral B cations are disordered, and magnetic susceptibility data indicate that cerium is present solely as Ce^{IV} in this phase. Crystal data: M_r = 719.78, orthorhombic, *Pbnm* (No. 62), a = 6.2158 (3) Å, b = 6.1793 (3) Å, c = 8.7286 (4) Å, V = 335.25 (3) Å^3, Z = 2, R_p = 6.92%, R_{wp} = 8.64%, χ^2 = 1.22. Ba_2PrBiO_6 shows ~75% ordering of the Pr^{III}/Pr^{IV} and Bi^{III}/Bi^{V} cations over two sites. This phase shows temperature-independent paramagnetism. Crystal data: M_r = 718.03, monoclinic, *I2/m* (No. 12), a = 6.2011 (2) Å, b = 6.1583 (2) Å, c = 8.6968 (3) Å, β = 89.922 (5)°, V = 332.12 (2) Å^3, Z = 2, R_p = 7.87%, R_{wp} = 10.04%, χ^2 = 1.13. Ba_2NdBiO_6 contains fully ordered Nd^{III} and Bi^{V} and is paramagnetic between 4.2 and 300 K. Crystal data: M_r = 723.90, monoclinic, *I2/m* (No. 12), a = 6.1776 (2) Å, b = 6.1366 (2) Å, c = 8.6686 (3) Å, β = 89.801 (2)°, V = 328.62 (3) Å^3, Z = 2, R_p = 3.12%, R_{wp} = 4.34%, χ^2 = 1.28. Paramagnetic Ba_2TbBiO_6 contains a mixture of Tb^{III} and Tb^{IV} at the terbium site and Bi^{III} and Bi^{V} at the bismuth site. Crystal data: M_r = 738.58, monoclinic, *I2/m* (No. 12), a = 6.1104 (2) Å, b = 6.0813 (3) Å, c = 8.5922 (4) Å, β = 89.97 (2)°, V = 319.28 (2) Å^3, Z = 2, R_p = 6.76%, R_{wp} = 8.53%, χ^2 = 1.06. Ba_2YbBiO_6 contains Yb^{III} on one octahedral site and Bi^{V} on the other. Crystal data: M_r = 752.69, trigonal $R\bar{3}$ (No. 148), a = 6.0252 (2) Å, α = 60.037 (2)°, V = 154.797 (1) Å^3, Z = 1, R_p = 4.71%, R_{wp} = 5.90%, χ^2 = 1.87.

Introduction

The Ba_2MBiO_6 (M = La to Lu) series of double perovskites was first prepared by Shuvaeva and Fesenko,[1] who found simple cubic perovskite-type unit cells, with a ≈ 4.3 Å, for the whole series, on the basis of X-ray powder diffraction data. This primitive-cubic unit cell implied that no octahedral B-cation ordering or octahedral tilting/distortions occurred for any members of this series.[2]

Since the discovery of superconductivity in $BaBi_{1-x}Pb_xO_3$,[3] $Ba_{1-x}K_xBiO_3$,[4,5] and layered cuprates based on the perovskite motif,[6,7] many perovskites containing bismuth have undergone intensive reinvestigations using state-of-the-art experimental methods. Phases such as $BaBiO_3$[8] itself, which contains both Bi^{III} and Bi^{V} and therefore should be formulated as $Ba_2Bi^{III}Bi^{V}O_6$,[9,10] show complex structural changes as a function of temperature, pressure, and chemical substitutions.[11–13] Recent studies[14,15] on the some members of the Ba_2MBiO_6 series have indicated structural behavior more complex than that of the simple cubic ABO_3 structures originally proposed: A detailed knowledge of the structures of these phases is essential in order to understand their physical properties. The best way to study subtle structural changes in $A_2B_2O_6$ phases is by single-crystal

† University of Houston.
‡ AT&T Bell Laboratories.
§ Present address: Department of Chemistry, Princeton University, Princeton, NJ 08544.
⊥ Present address: Department of Chemistry, University of Western Australia, Nedlands, WA 6907, Australia.
⊗ Abstract published in *Advance ACS Abstracts,* October 1, 1995.
(1) Shuvaeva, E. T.; Fesenko, E. G. *Kristallografiya* **1969**, *14*, 1066.
(2) Anderson, M. T.; Greenwood, K. B.; Taylor, G. A.; Poeppelmeier, K. R. *Prog. Solid State Chem.* **1993**, *22*, 197.
(3) Sleight, A. W.; Gillson, J. L.; Bierstedt, P. E. *Solid State Commun.* **1975**, *17*, 27.
(4) Cava, R. J.; Batlogg, B.; Krajewski, J. J.; Farrow, R. C.; Rupp, L. W. J.; White, A. E.; Short, K. T.; Peck, W. F. J.; Kometani, T. V. *Nature (London)* **1988**, *332*, 814.
(5) Hinks, D. G.; Dabrowski, B.; Jorgensen, J. D.; Mitchell, A. W.; Richards, D. R.; Pei, S.; Shi, D. *Nature (London)* **1988**, *333*, 836.
(6) Bednorz, J. G.; Müller, K. A. *Z. Phys.* **1986**, *B64*, 189.
(7) Wu, M. K.; Ashburn, J. R.; Torng, C. J.; Hor, P. H.; Meng, R. L.; Gao, L.; Huang, Z. J.; Wang, Y. Q.; Chu, C. W. *Phys. Rev. Lett.* **1987**, *58*, 908.
(8) Cox, D. E.; Sleight, A. W. *Solid State Commun.* **1976**, *19*, 969.
(9) Thornton, G.; Jacobson, A. J. *Acta Crystallogr.* **1978**, *B34*, 351.
(10) Chaillout, C.; Santoro, A.; Remeika, J. P.; Cooper, A. S.; Espinosa, G. P. *Solid State Commun.* **1988**, *65*, 1363.
(11) Reis, K. P.; Jacobson, A. J.; Nicol, J. M. J. *Solid State Chem.* **1993**, *107*, 428.
(12) Reis, K. P.; Jacobson, A. J.; Kulik, J. *Chem. Mater.* **1993**, *5*, 1070.
(13) Licheron, M.; Gervais, F.; Coutures, J.; Choisnet, J. *Solid State Commun.* **1990**, *75*, 759.
(14) Lenz, A.; Müller-Buschbaum, H. K. *J. Less-Common Met.* **1990**, *161*, 141.
(15) Beyerlein, R. A.; Jacobson, A. J.; Poeppelmeier, K. R. *J. Chem. Soc., Chem. Commun.* **1988**, 225.

0897-4756/95/2807-2161$09.00/0

methods:[2] If single crystals are not available, then powder X-ray diffraction methods often yield useful information on the ordering of the octahedral *cations*. Powder neutron diffraction data are required in order to reliably ascertain the detailed nature of the oxygen atom geometries in these phases.

In this paper we describe the solid-state synthesis and structural characterization by powder X-ray diffraction of the series of perovskite phases Ba_2MBiO_6 (M = Ce to Lu). The crystal structures of five members of the Ba_2MBiO_6 series (M = Ce, Pr, Nd, Tb, Yb) have been determined by Rietveld refinement of powder neutron diffraction data. Magnetic susceptibility data are reported for the compounds with M = Ce, Pr, Nd, and Tb.

Experimental Section

Synthesis. All the compounds in the series Ba_2MBiO_6 (M = La to Lu) were prepared by standard high-temperature ceramic methods. Stoichiometric mixtures of Bi_2O_3, $BaCO_3$, and the appropriate rare-earth oxide were thoroughly ground and heated in air in alumina crucibles at 800 °C (1 day), 900 °C (1 day), and 1000 °C (3–5 days), with intermediate regrindings. In each case, a dense black or dark brown powder resulted. The oxygen content of the praseodymium and terbium oxides was determined prior to reaction by thermogravimetric reduction in a 5% H_2/N_2 mixture and showed the presence of Pr_6O_{11} and Tb_4O_7, respectively. X-ray powder diffraction data for each phase were recorded at room temperature using a Scintag XDS2000 automated diffractometer (Cu Kα radiation, λ = 1.5418 Å, flat-plate sample, θ–θ scan mode).

Neutron Powder Diffraction. Constant-wavelength powder neutron diffraction data for Ba_2CeBiO_6, Ba_2PrBiO_6, and Ba_2TbBiO_6 were collected using the 32-detector high-resolution diffractometer BT-1 at the National Institute of Standards and Technology (NIST), Gaithersburg. Samples (~10 g) were enclosed in cylindrical aluminum sample cans, and a neutron wavelength of 1.540 Å was selected, as calibrated with alumina powder. Each data set was collected over a 12-h period (step size = 0.05°) and collated using in-house software into one overall bank (15° < 2θ < 130°) for analysis.

Time-of-flight neutron powder diffraction data for Ba_2NdBiO_6 and Ba_2YbBiO_6 were collected on the diffractometer SEPD at the Intense Pulsed Neutron Source (IPNS), Argonne National Laboratory. Samples were sealed into cylindrical vanadium sample cans, and room-temperature data were accumulated over ~12-h periods. After data reduction, the ±145° and ±90° scattering-angle data were used in the Rietveld refinements.

X-ray Rietveld Refinements. The initial refinements for the complete Ba_2MBiO_6 series were performed against the powder X-ray data sets, using the program GSAS.[16] All the powder patterns, except that of Ba_2CeBiO_6, showed a (111) line (indexing based on a double-pseudocube ~8.6 Å unit-cell edge), characteristic of rock-salt type B-cation ordering in perovskites[2] (Figure 1). Satisfactory profile fits were obtained using various crystallographic models of known $A_2B_2O_6$-type double-perovskite structures (cubic, orthorhombic, or monoclinic symmetries).[2] Fair precision was attained in the refinement of the lattice parameters and the heavy-atom positional/thermal parameters, but minimal information regarding the behavior of the oxygen atoms could be obtained from the X-ray profile refinements.

Neutron Rietveld Refinements. Visual examination of the neutron powder data confirmed that Ba_2CeBiO_6, Ba_2PrBiO_6, Ba_2NdBiO_6, and Ba_2TbBiO_6 adopt noncubic structures. Initially, these structures were fitted by trial-and-error, and various known distortion models (supercells) were used to fit to all the observed peak positions, as described by Poeppelmeier et al.[2] In each case, various crystallographic models

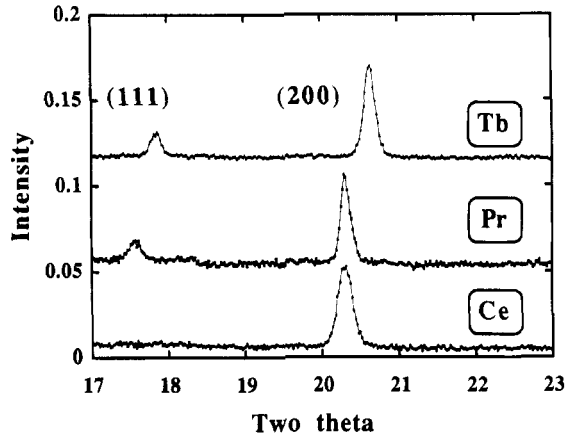

Figure 1. Sections of the low-angle X-ray powder patterns for Ba_2CeBiO_6, Ba_2PrBiO_6, and Ba_2TbBiO_6, showing the presence of the pseudocubic ($a \approx 8.6$ Å) (111) reflection for the Pr and Tb compounds, indicating that B-cation ordering has occurred for these two materials. Conversely, the absence of this reflection for Ba_2CeBiO_6 indicates that the B cations are disordered in this phase.

were tried, and the best fit was determined according to the criteria outlined below. The Ba_2CeBiO_6 data were fitted by an orthorhombic supercell, and the Ba_2PrBiO_6, Ba_2NdBiO_6, and Ba_2TbBiO_6 data were best modeled by a monoclinic unit cell. The Ba_2YbBiO_6 data appeared metrically cubic. The regions of the diffraction profile corresponding to scattering from the aluminum sample can were excluded from the Ba_2CeBiO_6, Ba_2PrBiO_6, and Ba_2TbBiO_6 refinements. The following coherent neutron scattering lengths ($\times 10^{-12}$ cm) were assigned: b(Ba) = 0.525, b(Ce) = 0.484, b(Pr) = 0.445, b(Nd) = 0.769, b(Tb) = 0.738, b(Yb) = 1.240, b(Bi) = 0.853, and b(O) = 0.581. Once a unit cell was established, the various profile (unit cell, zero-point, peak shape, background descriptors) and atomic positional and thermal parameters were added to the models as variables in the usual way, as the refinements progressed. For all these materials, an absorption correction was optimized in the latter stages of refinement, resulting in a significant improvement in fit and more realistic thermal parameters.

The best profile fit for the Ba_2CeBiO_6 data was obtained in the orthorhombic space group *Pbnm* (No. 62), with an approximate $\sqrt{2}a_p \times \sqrt{2}a_p \times 2a_p$ (a_p = nominal primitive-cubic cell length ≈ 4.3 Å) unit cell. This model assumes a completely random B-cation arrangement and is commonly observed for simple ABO_3 perovskites,[17] as well as for disordered $A_2B_2O_6$ double perovskite phases. This model is consistent with the *absence* of the double-pseudocubic (111) reflection in the powder X-ray data.[2] Final cell parameters of a = 6.2158 (3) Å, b = 6.1793 (3) Å, c = 8.7286 (4) Å (V = 335.25 (3) Å^3) were obtained (esd's in parentheses). Residuals of R_p = 6.92%, R_{wp} = 8.64% (χ^2 = 1.22) resulted, and the final observed, calculated, and difference profile plots for Ba_2CeBiO_6 are shown in Figure 2.

To model all the observed line positions, the Ba_2PrBiO_6, Ba_2NdBiO_6, and Ba_2TbBiO_6 data required monoclinic cells, with approximate dimensions $\sqrt{2}a_p \times \sqrt{2}a_p \times 2a_p$, with $\beta \sim 90°$. This unit cell corresponds to two known types of $A_2B_2O_6$-type perovskite structure: the $P2_1/n$ structure, exemplified by Ca_2CrTaO_6[18] or the $I2/m$ structure, exemplified by Ba_2BiO_6[8] (i.e., $Ba_2Bi^{III}Bi^{V}O_6$). Both the primitive and I-centered models were exhaustively tested for all three materials.

The $I2/m$ (nonstandard setting of $C2/m$, No. 12) body-centered model[8] was chosen for Ba_2PrBiO_6, Ba_2NdBiO_6, and Ba_2TbBiO_6, based on the following criteria: There was no observable intensity at any of the possible primitive reflections (those with hkl; $h + k + l \neq 2n$) for any of these materials. The $P2_1/n$ models, which have three crystallographically

(16) Larson, A. C.; Von Dreele, R. B. GSAS User Guide, Los Alamos National Laboratory, New Mexico, 1990.

(17) Geller, S. *J. Chem. Phys.* **1956**, *24*, 1236.

(18) Choy, J.-H.; Park, J.-H.; Hong, S.-T.; Kim, D.-K. *J. Solid State Chem.* **1994**, *111*, 370.

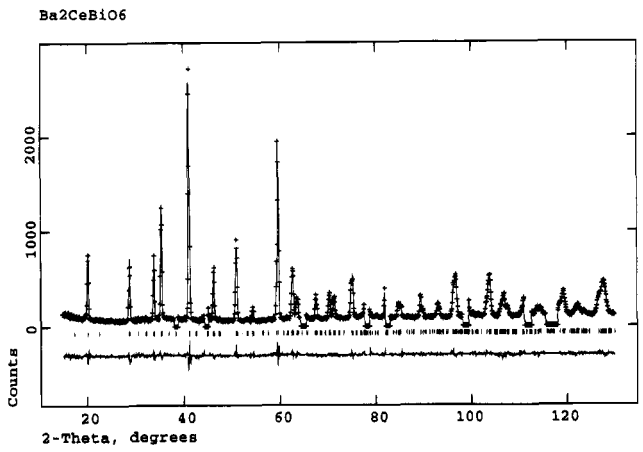

Figure 2. Final observed (crosses), calculated (line), and difference profiles for the Rietveld refinement of Ba_2CeBiO_6. Allowed reflection positions are indicated by tick marks.

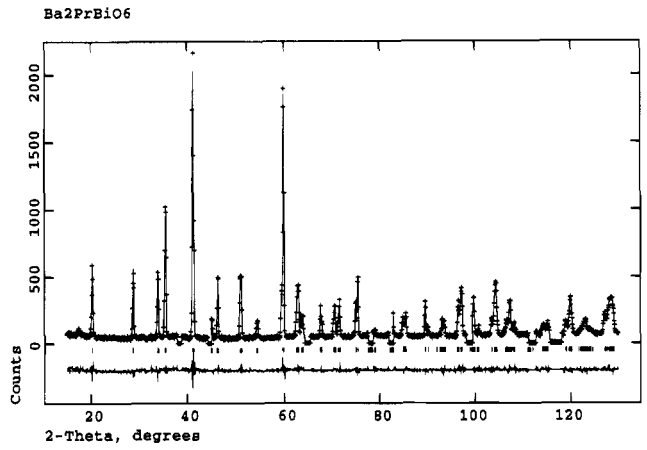

Figure 3. Final observed (crosses), calculated (line), and difference profiles for the Rietveld refinement of Ba_2PrBiO_6. Allowed reflection positions are indicated by tick marks.

independent oxygen atoms, were unstable and oscillatory with respect to the oxygen positional and thermal parameters, indicating that the primitive model was probably too low in symmetry. The *I*2/*m* models rapidly converged, without any pseudosymmetry effects. Finally, the *I*2/*m* models refined to virtually identical residuals to the $P2_1/n$ models, but with significantly fewer variable parameters.

For Ba_2PrBiO_6, a = 6.2011 (2) Å, b = 6.1583 (2) Å, c = 8.6968 (3) Å, β = 89.922 (5)° (V = 332.12 (2) Å^3), with R_p = 7.87%, R_{wp} = 10.04% (χ^2 = 1.13). Final profile plots for Ba_2PrBiO_6 are shown in Figure 3. For Ba_2NdBiO_6, a = 6.1776 (2) Å, b = 6.1366 (2) Å, c = 8.6686 (3) Å, β = 89.801 (2)° (V = 328.62 (3) Å^3). Residuals of R_p = 3.12%, R_{wp} = 4.34% (χ^2 = 1.28) resulted (profile plots shown in Figure 4). For Ba_2TbBiO_6, a = 6.1104 (2) Å, b = 6.0813 (3) Å, c = 8.5922 (4) Å, β = 89.97 (2)° (V = 319.28 (2) Å^3), R_p = 6.76%, R_{wp} = 8.53%, χ^2 = 1.06, profile plots in Figure 5.

Both the neutron and X-ray data for Ba_2YbBiO_6 appeared metrically cubic, with $a = 2a_p$, indicative of an undistorted, rock-salt ordered, $A_2B_2O_6$ perovskite (probable space group $Fm\bar{3}m$). However, refinements based on such a model resulted in poor profile fits, high residuals, and physically unreasonable thermal parameters for the oxygen atom species. Therefore, various distorted models which maintained Yb/Bi *B*-cation order were tried. The *I*2/*m* model used for the Pr, Nd, and Tb Ba_2MBiO_6 phases was unsuccessful for Ba_2YbBiO_6 and resulted in unstable, oscillatory refinements, indicating that monoclinic symmetry was too low. A crystallographic model was developed in space group $R\bar{3}$ (No. 148), which allows for *B*-cation order and is an allowed subgroup of the undistorted $Fm\bar{3}m$ double cubic structure. After damped refinement cycles, this model converged satisfactorily to a = 6.0252 (2) Å, α = 60.037 (2)°, V = 154.797 (1) Å^3, R_p = 4.71%, R_{wp} = 5.90% (χ^2 = 1.87), with final profile plots shown in Figure 6.

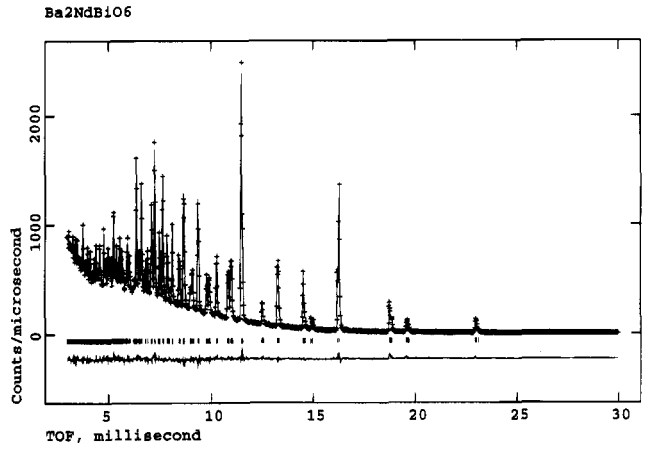

Figure 4. Final observed (crosses), calculated (line), and difference profiles for the Reitveld refinement of Ba_2NdBiO_6 (time-of-flight neutron powder data). Allowed reflection positions are indicated by tick marks.

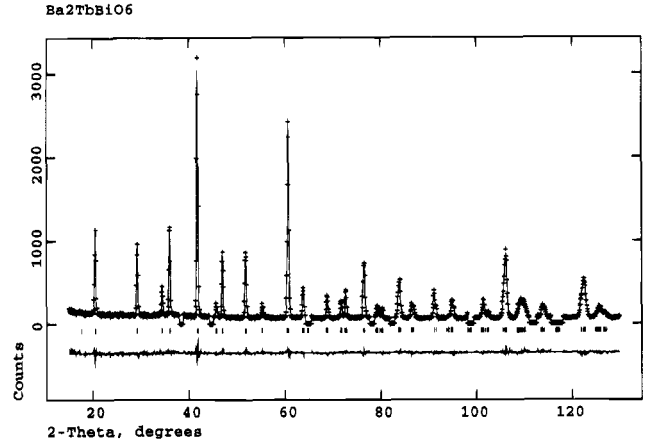

Figure 5. Final observed (crosses), calculated (line), and difference profiles for the Reitveld refinement of Ba_2TbBiO_6. Allowed reflection positions are indicated by tick marks.

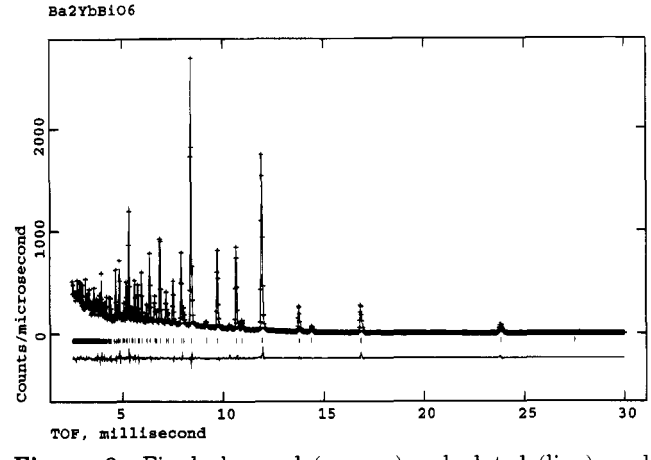

Figure 6. Final observed (crosses), calculated (line), and difference profiles for the Reitveld refinement of Ba_2YbBiO_6 (time-of-flight neutron powder data). Allowed reflection positions are indicated by tick marks.

Magnetic Measurements. Magnetic susceptibility measurements were made for four of the Ba_2MBiO_6 compounds (M = Ce, Pr, Nd, Tb). Susceptibilities were measured on polycrystalline samples from 4.2 to 300 K using the Faraday technique, as described elsewhere.[19] The relative accuracy of χ_g is approximately $\pm 1 \times 10^{-10}$ emu/g or less, depending on the sample size, but the absolute accuracy of the susceptibility, relative to several known standards, is ~±2%.

(19) DiSalvo, F. J.; Waszczak, J. V. *Phys. Rev.* **1981**, *B23*, 457.

Table 1. Properties of Ba_2MBiO_6 Series

M	r^a	color	O content[b]	symmetry[c]	a^d
La	1.172			monoclinic	8.767[e]
Ce	1.15/1.01	black	6.00	orthorhombic	8.752/8.7526
Pr	1.13/0.99	black	6.00	monoclinic	8.728/8.7251
Nd	1.123	brown	5.99	monoclinic	8.697/8.6944
Sm	1.098	brown	5.96	monoclinic	8.666
Eu	1.087	brown	6.01	monoclinic	8.638
Gd	1.078	brown	5.99	monoclinic	8.634
Tb	1.063	black	6.02	monoclinic	8.602/8.6112
Dy	1.052	brown	5.99	monoclinic	8.589
Ho	1.041	brown	5.97	monoclinic	8.577
Er	1.030	brown	6.00	monoclinic	8.566
Yb	1.008	brown	6.00	rhombohedral	8.531/8.5233
Lu	1.001	brown	5.94	cubic	8.533

[a] Crystal radius (Å) for the Ln^{III} cation in octahedral coordination. If two values are given, the first applies to the Ln^{III} species, the second to Ln^{IV}. Comparable values for bismuth: Bi^{III} 1.17 Å, Bi^{V} 0.90 Å (see ref 26). [b] Determined by chemical analysis. [c] From X-ray or neutron Rietveld refinements. [d] Equivalent pseudocubic cell edge (Å, see text). If two values are given, the first refers to the X-ray refinement, the second to the neutron refinement. [e] Data provided by K. R. Poeppelmeier.

Oxygen Content. The oxidizing powers of the Ba_2MBiO_6 samples were determined by iodometric titration. Typically, 100–120 mg of oxide was dissolved under a nitrogen purge in 15 mL of 1.2 M HCl and 5 mL of water containing 1.2 g of KI. The liberated iodine was determined by titration with 0.1 M sodium thiosulfate solution using a redox electrode to determine the end point. The oxygen stoichiometries were then calculated assuming a Ba:*M*:Bi ratio of 2:1:1, corresponding to the stoichiometries used in the preparations and consistent with the neutron diffraction results. Determinations were carried out in triplicate and the error on the composition is estimated to be better than ±0.01. Final calculated stoichiometries are listed in Table 1.

Results

Structures of Ba_2MBiO_6 Series. All the compounds of the Ba_2MBiO_6 series crystallize as $A_2B_2O_6$ perovskite-type structures. A smooth, roughly linear decreasing trend in unit-cell size (Table 1), which is consistent with the decreasing ionic radius of the rare-earth cations across the series, is observed. The equivalent value for monoclinic Ba_2LaBiO_6[20] is also consistent with this trend.

Magnetism. Ba_2CeBiO_6 is diamagnetic, with a small Curie component at low temperature that is most likely associated with the presence of a small amount of impurities or defects. These data indicate that cerium is all in the Ce^{IV} (f^0) oxidation state and that by the charge-balancing criterion, the bismuth atoms in Ba_2CeBiO_6 must be present as an equal mixture of Bi^{III} and Bi^{V} cations.

The magnetic susceptibility data for Ba_2PrBiO_6 (Figure 7) show unusual behavior. The low-temperature data indicate the presence of a small paramagnetic Curie contribution that corresponds to an effective moment of 0.56 μ_B. This value is much smaller than the expected values calculated either for f^2-Pr^{III} (3.58 μ_B) or f^1-Pr^{IV} (2.54 μ_B), using the relationship $\mu_{eff} = [gJ(J+1)]^{1/2}$. We have assumed that this moment represents a contribution from defects and have subtracted it from the data using the standard procedure of fitting to the low-temperature region where the Curie term makes a significant contribution. Fitting the data in the range 4.2–80 K using $\chi_g = C_g/(T-\theta) + \chi_0$ gave values of 54.8 $\times$ 10^{-6} emu/g K, 4.7 $\times$ 10^{-6} emu/g, and −6 K for C_g, χ_0, and θ, respectively. After subtraction of the Curie term, a nearly temperature-independent paramagnetic contribution of (4–5) $\times$ 10^{-6} emu/g remains. A similar procedure was used to analyze the Ba_2CeBiO_6 data (vide supra). In this case, the defect concentration is lower (0.2 μ_B), and after subtraction, a temperature-independent diamagnetic component remains.

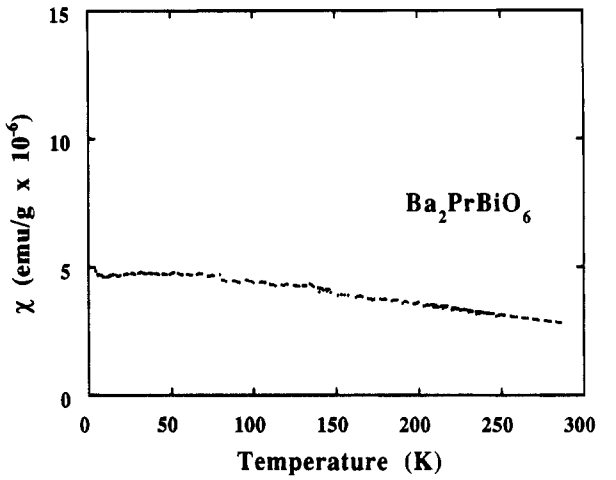

Figure 7. Plot of inverse magnetic susceptibility versus temperature for Ba_2PrBiO_6.

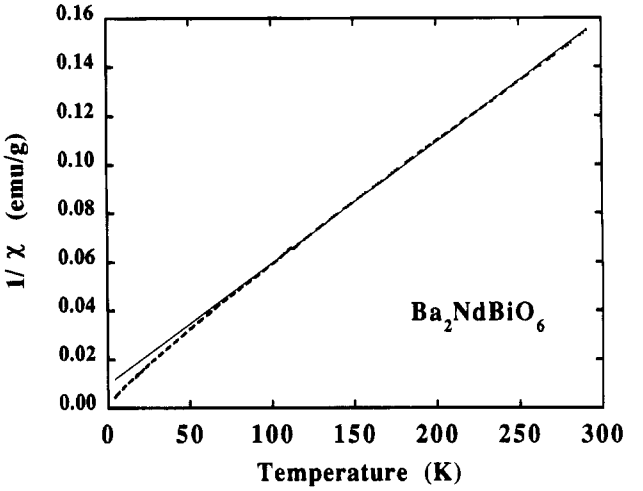

Figure 8. Plot of inverse magnetic susceptibility versus temperature for Ba_2NdBiO_6.

The magnetic susceptibility data for Ba_2NdBiO_6 are plotted in Figure 8 as $1/\chi_g$ versus temperature. The data show Curie–Weiss behavior, except for a small deviation at low temperature, possibly due to crystal field effects. A fit to the data in the range 75–300 K gave a Curie constant of 0.6903 emu/mol K and θ = −13 K. The effective magnetic moment calculated from the Curie constant is 3.40 μ_B compared with a calculated value of 3.62 μ_B for Nd^{III} (f^3).

The magnetic susceptibility data for Ba_2TbBiO_6 ($1/\chi_g$ versus T) are plotted in Figure 9. These data also show Curie–Weiss behavior over the whole temperature range. A fit to the data over the range 25–300 K gave values of 13.57 $\times$ 10^{-3} emu/g K for C_g, −2.05 $\times$ 10^{-6} emu/g for χ_0, and −21 K for θ. The Curie constant equates to an effective terbium magnetic moment of 8.95 μ_B, intermediate between the predicted values of 9.72 μ_B and 7.94 μ_B for Tb^{III} (f^8) and Tb^{IV} (f^7), respectively.

Structure of Ba_2CeBiO_6. Final atomic positional and thermal parameters for Ba_2CeBiO_6 are listed in Table 2, with selected geometrical data given in Table

(20) Poeppelmeier, K. R. Unpublished results.

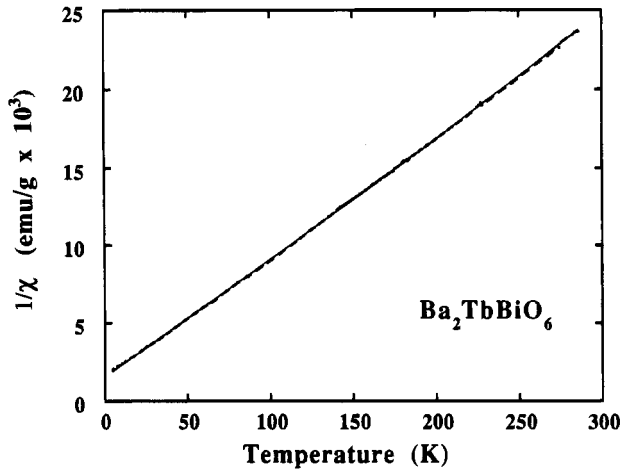

Figure 9. Plot of inverse magnetic susceptibility versus temperature for Ba_2TbBiO_6.

Table 2. Atomic Positional/Thermal Parameters for Ba_2CeBiO_6

atom	x	y	z	U_{iso} (Å²)
Ba(1)	0.5046 (8)	−0.007 (2)	1/4	0.0131 (7)
Ce/Bi(1)	0	0	0	0.060 (5)
O(1)	0.0653 (6)	0.001 (3)	1/4	0.0190[a]
O(2)	0.2358 (7)	0.262 (2)	−0.0339 (3)	0.0272[a]

[a] U_{eq} (Å²) = $(U_1U_2U_3)^{1/3}$.

3. Ba_2CeBiO_6 crystallizes as a orthorhombically distorted perovskite, with random cerium/bismuth occupancy of the single crystallographic octahedral B site. This type of supercell results from nominal rotations of the BO_6 octahedra about the $[011]_{cubic}$ and $[100]_{cubic}$ axes, and is termed an $a^+b^-b^-$ distortion in Glazer's notation.[21]

The Ba cation in Ba_2CeBiO_6 is irregular 12-coordinate, with d_{av}(Ba−O) = 3.105 (3) Å. The spread of Ba−O bond distances [2.731 (6) to 3.422 (6) Å] covers 0.69 Å. Because of the B-site disorder, only an average value of the Ce/Bi−O bond distance can be obtained. The measured value of 2.216 (3) Å is consistent with values of 2.24 and 2.23 Å calculated from ionic radii assuming formal oxidation state distributions of Ce^{III}/Bi^{V} (1:1 ratio) and $Ce^{IV}/Bi^{III}/Bi^{V}$ (2:1:1 ratio), respectively. However, magnetic susceptibility data for Ba_2CeBiO_6 (vide supra) definitively indicate the presence of only Ce^{IV} in this phase.

Structure of Ba_2PrBiO_6. Final atomic positional and thermal parameters for Ba_2PrBiO_6 are listed in Table 4, with selected geometrical data in Table 5. Ba_2PrBiO_6 crystallizes in an I-centered monoclinic unit cell, with two crystallographically distinct B cation sites. This supercell results from rotations of the BO_6 octahedra about the $[011]_{cubic}$ axis ($a^0b^-b^-$ tilts in Glazer's notation). The Ba cation in Ba_2PrBiO_6 is irregular 12-coordinate, with d_{av}(Ba−O) = 3.095 (3) Å.

An unconstrained refinement, which simply allowed the Pr and Bi site-occupancy factors to vary, indicated partial disorder of the Pr and Bi sites. Further cycles of constrained refinement, such that the overall 1:1 Pr-to-Bi ratio was maintained, indicated that the Pr site contained 25 (3)% Bi, and vice versa. Average bond distances of d_{av} = 2.267 (4) Å for the predominant Pr site and d_{av} = 2.146 (4) Å for the predominant Bi site resulted from the refinement. The magnetic susceptibility data for Ba_2PrBiO_6 show temperature-independent paramagnetism.

The measured Pr−O and Bi−O bond distances are significantly different from the values calculated from ionic radii for Pr^{III}−O (2.34 Å) and Bi^{V}−O (2.11 Å), suggesting that a simple Pr^{III}/Bi^{V} model is inadequate to describe the true valence situation in Ba_2PrBiO_6. The absence of a localized moment corresponding in magnitude to the expected values for either Pr^{III} or Pr^{IV} (vide supra) suggests an unusual valence situation in this compound that warrants further study.

Structure of Ba_2NdBiO_6. This material is isostructural with Ba_2PrBiO_6, but unconstrained refinements indicated that negligible site mixing of the Nd and Bi species was occurring, and the final cycles of least squares modeled these sites as being completely ordered. Final atomic positional/thermal parameters and geometrical data for Ba_2NdBiO_6 are presented in Tables 6 and 7, respectively, and the Ba_2NdBiO_6 structure is show in Figure 10.

The average bond distances of d_{av} = 2.299 (1) Å for the Nd site and d_{av} = 2.093 (1) Å for the Bi site are in good agreement with those expected from ionic-radius sums, assuming the presence of Nd^{III} and Bi^{V} at the two sites: $d_{calc}(Nd^{III}-O)$ = 2.33 Å; $d_{calc}(Bi^{V}-O)$ = 2.11 Å. This Nd^{III}/Bi^{V} oxidation state distribution is understandable, since Nd^{IV} is rare in simple solid materials. The barium cation is irregular 12-coordinate in Ba_2NdBiO_6, with d_{av}(Ba−O) = 3.084 (1) Å (min = 2.739 (3) Å, max = 3.444 (3) Å).

The susceptibility data for Ba_2NdBiO_6 described above confirm the presence of Nd^{III} in this material.

Structure of Ba_2TbBiO_6. Like Ba_2CeBiO_6 and Ba_2NdBiO_6, this material crystallizes in space group $I2/m$. Unconstrained site-population refinements indicated that negligible site mixing of the Tb and Bi species was occurring, and the final cycles of least-squares modeled these sites as being completely ordered. We note, however, that the scattering-length contrast between Tb and Bi is relatively small. Final atomic positional/thermal parameters and geometrical data for Ba_2TbBiO_6 are presented in Tables 8 and 9, respectively.

The barium cation in Ba_2TbBiO_6 is 12-coordinate with d_{av}(Ba−O) = 3.084 (1) Å, which is vey similar to the equivalent species in Ba_2NdBiO_6 and Ba_2PrBiO_6. An average bond distance of 2.177 (5) Å for the Tb site and 2.159 (5) Å for the Bi site result. Assuming the presence of pure Tb^{III} and Bi^{V} at these two sites, ionic-radii sums would yield d_{calc} values of 2.27 and 2.11 Å, respectively. Thus, the actual valence situation in Ba_2TbBiO_6 appears to be more complex than a simple Tb^{III}/Bi^{V} pairing. We note that the observed Tb−O distance is roughly intermediate between those expected for Tb^{III}−O (2.27 Å) and Tb^{IV}−O (2.11 Å), based on ionic radii sums.

The observed magnetic moment per terbium atom in Ba_2TbBiO_6 lies between the predicted values for Tb^{III} and Tb^{IV}.

Structure of Ba_2YbBiO_6. This phase crystallizes in the trigonal space group $R\bar{3}$ (No. 148), with no detectable Yb/Bi disorder. Final atomic positional/thermal parameters and geometrical data for Ba_2YbBiO_6 are given in Tables 10 and 11, respectively. The observed Yb−O and Bi−O bond distances [2.180 (2) and 2.092 (2) Å, respectively] are in good accord with those expected for Yb^{III} (2.22 Å) and Bi^{V} (2.11 Å), which is the only chemically reasonable metal valence distribution for this com-

(21) Glazer, A. M. *Acta Crystallogr.* **1975**, *A31*, 756.

Table 3. Bond Distances (Å)/Angles (deg) for Ba_2CeBiO_6

Ba(1)–O(1)	2.731 (6)	Ba(1)–O(1)	3.485 (6)
Ba(1)–O(1)	3.07 (2)	Ba(1)–O(1)	3.17 (2)
Ba(1)–O(2) × 2	3.422 (6)	Ba(1)–O(2) × 2	3.225 (6)
Ba(1)–O(2) × 2	2.813 (9)	Ba(1)–O(2) × 2	2.940 (9)
Ce/Bi(1)–O(1) × 2	2.2196 (7)	Ce/Bi(1)–O(2) × 2	2.205 (6)
Ce/Bi(1)–O(2) × 2	2.223 (6)		
O(1)–Ce/Bi(1)–O(1)	180	O(1)–Ce/Bi(1)–O(2)	90.4 (3)
O(1)–Ce/Bi(1)–O(2)	89.9 (3)	O(1)–Ce/Bi(1)–O(2)	89.6 (3)
O(1)–Ce/Bi(1)–O(2)	90.1 (3)	O(2)–Ce/Bi(1)–O(2)	88.67 (3)
O(2)–Ce/Bi(1)–O(2)	91.33 (3)	O(2)–Ce/Bi(1)–O(2)	180
Ce/Bi(1)–O(1)–Ce/Bi(1)	158.9 (2)	Ce/Bi(1)–O(2)–Ce/Bi(1)	163.5 (2)

Table 4. Atomic Positional/Thermal Parameters for Ba_2PrBiO_6

atom	*x*	*y*	*z*	U_{iso} (Å^2)
Ba(1)	0.5036 (7)	1/2	0.250 (2)	0.014 (6)
Pr(1)	1/2	0	0	0.0047 (5)
Bi(1)	0	1/2	0	0.0047 (5)
O(1)	0.2421 (9)	0.254 (2)	−0.0334 (3)	0.0237[a]
O(2)	0.4361 (6)	0	0.2589 (9)	0.0145[a]

[a] U_{eq} (Å^2) = $(U_1U_2U_3)^{1/3}$.

Table 5. Bond Distances (Å)/Angles (deg) for Ba_2PrBiO_6

Ba(1)–O(1) × 2	3.32 (2)	Ba(1)–O(1) × 2	2.88 (2)
Ba(1)–O(1) × 2	2.87 (2)	Ba(1)–O(1) × 2	3.30 (2)
Ba(1)–O(2) × 2	3.1085 (9)	Ba(1)–O(2)	2.728 (6)
Ba(1)–O(2)	3.475(6)		
Pr(1)–O(1) × 4	2.257 (8)	Pr(1)–O(2) × 2	2.286 (8)
Bi(1)–O(1) × 4	2.152 (8)	Bi(1)–O(2) × 2	2.134 (8)
O(1)–Pr(1)–O(1)	92.2 (5)	O(1)–Pr(1)–O(1)	180
O(1)–Pr(1)–O(1)	87.8 (5)	O(1)–Pr(1)–O(2)	90.3 (1)
O(1)–Pr(1)–O(2)	89.7 (1)	O(2)–Pr(1)–O(2)	180
O(1)–Bi(1)–O(1)	90.5 (5)	O(1)–Bi(1)–O(1)	180
O(1)–Bi(1)–O(1)	89.5 (5)	O(1)–Bi(1)–O(2)	89.9 (2)
O(1)–Bi(1)–O(2)	90.1 (2)	O(2)–Bi(1)–O(2)	180
Pr(1)–O(1)–Bi(1)	164.8 (2)	Pr(1)–O(2)–Bi(1)	159.3 (2)

Table 6. Atomic Positional/Thermal Parameters for Ba_2NdBiO_6

atom	*x*	*y*	*z*	U_{iso} (Å^2)
Ba(1)	0.5032 (4)	1/2	0.2511 (4)	0.011 (2)
Nd(1)	1/2	0	0	0.0040 (3)
Bi(1)	0	1/2	0	0.0035 (3)
O(1)	0.2362 (3)	0.2596 (4)	−0.0315 (2)	0.0168[a]
O(2)	0.4397 (3)	0	0.2627 (3)	0.0138[a]

[a] U_{eq} (Å^2) = $(U_1U_2U_3)^{1/3}$.

Table 7. Bond Distances (Å)/Angles (deg) for Ba_2NdBiO_6

Ba(1)–O(1) × 2	3.305 (4)	Ba(1)–O(1) × 2	2.893 (3)
Ba(1)–O(1) × 2	2.860 (4)	Ba(1)–O(1) × 2	3.258 (4)
Ba(1)–O(2) × 2	3.0949 (4)	Ba(1)–O(2)	2.739 (3)
Ba(1)–O(2)	3.444 (3)		
Nd(1)–O(1) × 4	2.296 (2)	Nd(1)–O(2) × 2	2.306 (2)
Bi(1)–O(1) × 4	2.093 (2)	Bi(1)–O(2) × 2	2.092 (2)
O(1)–Nd(1)–O(1)	92.1 (2)	O(1)–Nd(1)–O(1)	180
O(1)–Nd(1)–O(1)	87.9 (2)	O(1)–Nd(1)–O(2)	90.30 (4)
O(1)–Nd(1)–O(2)	89.70 (4)	O(2)–Nd(1)–O(2)	180
O(1)–Bi(1)–O(1)	90.3 (2)	O(1)–Bi(1)–O(1)	180
O(1)–Bi(1)–O(1)	89.7 (2)	O(1)–Bi(1)–O(2)	89.89 (5)
O(1)–Bi(1)–O(2)	90.11 (5)	O(2)–Bi(1)–O(2)	180
Nd(1)–O(1)–Bi(1)	165.62 (5)	Nd(1)–O(2)–Bi(1)	160.44 (8)

pound. The site symmetry ($\bar{3}$.) is the same for both the Yb and Bi species. The rhombohedral symmetry of this double perovskite is uncommon, but it is notable that a similar type of rhombohedral cell was required to model the high-temperature $Ba_{0.9}K_{0.1}BiO_3$ structure[22] and the structures of the "barium excess" perovskites $Ba_2[Ba_xBi_{1-x}]BiO_6$ (x = 0.22 and 0.28).[11] The Ba cation (site symmetry 3.) in Ba_2YbBiO_6 is 12-coordinate [d_{av}(Ba–O) = 3.017 (5) Å].

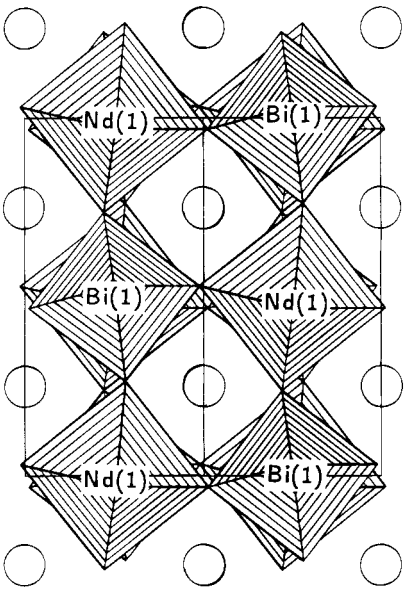

Figure 10. Polyhedral view down [110] of the Ba_2NdBiO_6 structure (space group *I*2/*m*), showing the ordering and alternation of the vertex-sharing NdO_6 and BiO_6 octahedra. Note the octahedral tilting effect and size differences between the bismuth and neodymium octahedra. Barium cations are represented by plain circles.

Table 8. Atomic Positional/Thermal Parameters for Ba_2TbBiO_6

atom	*x*	*y*	*z*	U_{iso} (Å^2)
Ba(1)	0.502 (2)	1/2	0.249 (3)	0.0105 (5)
Tb(1)	1/2	0	0	0.0021 (3)
Bi(1)	0	1/2	0	0.0021 (3)
O(1)	0.238 (2)	0.239 (2)	−0.0254 (5)	0.0146 (6)
O(2)	0.4534 (7)	0	0.252 (2)	0.012 (2)

Table 9. Bond Distances (Å)/Angles (deg) for Ba_2TbBiO_6

Ba(1)–O(1) × 2	3.27 (2)	Ba(1)–O(1) × 2	2.95 (2)
Ba(1)–O(1) × 2	2.82 (2)	Ba(1)–O(1) × 2	3.15 (2)
Ba(1)–O(2) × 2	3.0552 (8)	Ba(1)–O(2)	2.782 (8)
Ba(1)–O(2)	3.328 (8)		
Tb(1)–O(1) × 4	2.172 (8)	Tb(1)–O(2) × 2	2.19 (2)
Bi(1)–O(1) × 4	2.165 (8)	Bi(1)–O(2) × 2	2.15 (2)
O(1)–Tb(1)–O(1)	96.0 (4)	O(1)–Tb(1)–O(1)	180
O(1)–Tb(1)–O(1)	84.0 (4)	O(1)–Tb(1)–O(2)	90.2 (2)
O(1)–Tb(1)–O(2)	89.8 (2)	O(2)–Tb(1)–O(2)	180
O(1)–Bi(1)–O(1)	85.7 (4)	O(1)–Bi(1)–O(1)	180
O(1)–Bi(1)–O(1)	94.3 (4)	O(1)–Bi(1)–O(2)	89.4 (2)
O(1)–Bi(1)–O(2)	90.6 (2)	O(2)–Bi(1)–O(2)	180
Tb(1)–O(1)–Bi(1)	167.4 (2)	Tb(1)–O(2)–Bi(1)	164.9 (3)

(22) Pei, S.; Jorgensen, J. D.; Dabrowski, B.; Hinks, D. G.; Richards, D. R.; Mitchell, A. W.; Newsam, J. M.; Sinha, S. K.; Vaknin, D.; Jacobson, A. J. *Phys. Rev.* **1990**, *B41*, 4126.

Table 10. Atomic Positional/Thermal Parameters for Ba_2TbBiO_6

atom	x	y	z	U_{iso} (Å^2)
Ba(1)	0.2508 (15)	0.2508	0.2508	0.0100 (2)
Bi(1)	0	0	0	0.0044 (1)
Yb(1)	1/2	1/2	1/2	0.0044 (1)
O(1)	−0.2210 (4)	−0.2687 (4)	0.242 (2)	0.0102[a]

[a] U_{eq} (Å^2) = $(U_1U_2U_3)^{1/3}$.

Table 11. Bond Distances (Å)/Angles (deg) for Ba_2YbBiO_6

Ba(1)−O(1) × 3	2.871 (2)	Ba(1)−O(1) × 3	3.158 (2)
Ba(1)−O(1) × 3	3.01 (2)	Ba(1)−O(1) × 3	3.03 (2)
Yb(1)−O(1) × 6	2.180 (2)	Bi(1)−O(1) × 6	2.092 (2)
O(1)−Yb(1)−O(1)	90.9 (4)	O(1)−Yb(1)−O(1)	180
O(1)−Yb(1)−O(1)	89.1 (4)		
O(1)−Bi(1)−O(1)	89.4 (4)	O(1)−Bi(1)−O(1)	180
O(1)−Bi(1)−O(1)	90.6 (4)		
Yb(1)−O(1)−Bi(1)	172.21 (7)		

Discussion

We have prepared and characterized the Ba_2MBiO_6 (M = La to Lu) series of double perovskites. All these phases form compounds with stoichiometries close to $Ba_2MBiO_{6.00}$, according to the chemical analysis and neutron diffraction results. Contrary to the initial report[1] on these phases, most of them show octahedral B-cation order, and display distortions from cubic symmetry. The distortion decreases across the rare-earth series, from monoclinic Ba_2LaBiO_6[20] to cubic Ba_2LuBiO_6. This trend toward higher symmetry on crossing the lanthanide series may be correlated with the better fit of the barium cation in its 12-coordinate cavity for the smaller lanthanide ions in combination with Bi^{III}. This may be quantified by the Goldschmidt tolerance factor,[23] t, adapted to double perovskites:[2] the closer the tolerance factor is to 1.00, the more likely it is that a (double) perovskite will adopt undistorted cubic symmetry. Ba_2LaBiO_6[20] has a t value of 0.93 and is monoclinic, whereas Ba_2LuBiO_6 is metrically cubic and has t = 0.97.

When the lattice constant for each compound is expressed as a pseudocubic $2a$ value (vide infra), a smooth evolution from the largest value at La to the smallest at Lu is seen (decrease = 2.7%), typical of the "lanthanide contraction" effect seen in other isostructural lanthanide-containing series of compounds. This trend across the series in pseudocubic cell parameter is almost linear with respect to the sum of the average B-cation radius and the oxide anion radius, $r(B) + r(O)$, where $r(B)$ is the average radius of M^{III} and Bi^{V} (Figure 11). The cell parameters for Ba_2CeBiO_6 and Ba_2PrBiO_6 show some deviation from the general trend, possibly due to the Ce/Bi and Pr/Bi site mixing observed in these two compounds.

All the compounds studied containing M^{III} rare-earth ions have ordered B-cation distributions, and are well formulated as $Ba_2M^{III}Bi^{V}O_6$. This conclusion is based on successful Rietveld refinements using neutron data and chemically reasonable bond lengths for the two independent B-cation sites. However, when the rare-earth cation has a chemically accessible M^{IV} oxidation state (Ce, Pr, Tb), then more complex structural behavior is observed.

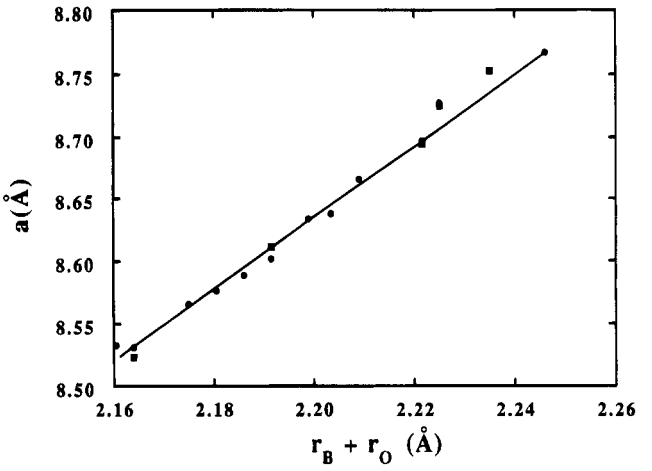

Figure 11. Variation of the lattice constants of the Ba_2MBiO_6 series with the average B−O bond distance (see text).

Ba_2CeBiO_6 has completely disordered B cations and adopts the orthorhombic $GdFeO_3$-type structure,[17] as observed for many simple ABO_3 perovskites, including the parent rare-earth phases $BaMO_3$ (M = Ce, Pr).[24] As described above, the magnetic data indicate that all the cerium is present as Ce^{IV}. A very recent study by Drost and Fu of the $BaCa_{1-x}Bi_xO_3$ solid solution[25] is in agreement with our results for the 50:50 Ce/Bi sample—these authors found that all $BaCe_{1-x}Bi_xO_3$ samples with $x < 0.8$ crystallized in the orthorhombic $GdFeO_3$ structure (disordered B cations).

Ba_2TbBiO_6 has negligible B-cation site mixing but intermediate oxidation states for both Tb and Bi. The average Tb−O bond distance obtained from the powder neutron refinement is intermediate between values calculated for Tb^{IV}−O and Tb^{III}−O bonds, based on ionic radii.

Ba_2PrBiO_6 is the most interesting case and shows B-cation site mixing. The site-mixing effect (neutron diffraction data) indicates about 25% Bi on the Pr site, and vice versa. The magnetic susceptibility of Ba_2PrBiO_6 is unusual, as the observed paramagnetic susceptibility is much less than that expected for either Pr^{III} or Pr^{IV}, and the susceptibility contains a significant temperature-independent component.

In conclusion, a combination of neutron powder diffraction and magnetic susceptibility measurements have been effective in elucidating the detailed structures of several members of the Ba_2MBiO_6 series of double perovskites. Further studies of the electronic properties of these compounds are in progress.

Acknowledgment. We thank Jim Richardson (ANL) and Jackie Nicol (NIST) for assistance with the neutron powder diffraction data collections. Ken Poeppelmeier (Northwestern) kindly shared his results on the Ba_2LaBiO_6 system with us prior to publication. This work is partly funded by the Robert A. Welch Foundation (Grant E-1207).

CM950244W

(23) Goldschmidt, V. M. *Str. Nor. Vidensk-Akad. Oslo* **1926**, *1*, 1.
(24) Jacobson, A. J.; Tofield, B. C.; Fender, B. E. F. *Acta Crystallogr.* **1972**, *B28*, 956.
(25) Drost, R. J.; Fu, W. T. *Mater. Res. Bull.* **1995**, *30*, 471.
(26) Shannon, R. D. *Acta Crystallogr.* **1976**, *A32*, 751.